Aalborg Universitet

Systematic Approach for Transient Stability Evaluation of Grid-Tied Converters during Power System Faults

Taul, Mads Graungaard; Wang, Xiongfei; Davari, Pooya; Blaabjerg, Frede

Systematic Approach for Transient Stability Evaluation of Grid-Tied Converters during Power System Faults

Mads Graungaard Taul, Xiongfei Wang, Pooya Davari, Frede Blaabjerg

Dept. of Energy Technology
Aalborg University
Aalborg, Denmark
mkg@et.aau.dk, xwa@et.aau.dk, pda@et.aau.dk, fbl@et.aau.dk

Abstract—Grid-tied converters subject to severe grid faults might experience transient instability and loss of synchronization. As studying this phenomenon deals with large-signal disturbances, a linearized equivalent will no longer be an accurate approximation of the system. Consequently, a highly used approach is to perform time-domain simulation studies of a detailed model of the system to assess the transient stability and overall performance. However, such an approach might result in a large computational burden and limited physical insight to the system. To address this issue, this paper presents a systematic approach to assess the transient stability of the inherently nonlinear problem alongside an methodology for setting the control parameters to avert transient instability. Using a simplified model for the converter, it is shown that phase-plane analysis is accurate for analyzing the transient synchronization stability. To that end, a critical damping ratio of the phase-locked loop can be found to identify the domain of attraction of the state trajectories, which has been experimentally verified. Using this together with an engineering insight to the system, one can set the controller parameters of the phase-locked loop such to guarantee stability during severe grid faults and perform worst-case planning settings for the controller and protection devices.

Index Terms—Grid-Connection, Voltage-Source Converter, Grid Fault, Transient Stability, Fault Ride-Through

I. Introduction

Renewable energy sources are usually interfaced with the power system through grid-connected converters controlled as grid-following structures injecting the harvested energy as active power to the grid. During a grid fault, the operating point of the converter must be altered to inject reactive current to support the low network voltage as required by the grid code [1]. However, during severe faults, the combination of the injected current level, grid impedance, and fault voltage magnitude may result in the power injection task of the converter to be statically unstable, leading to loss of synchronization of the Phase-Locked Loop (PLL) [2]–[4]. Moreover, even with the possibility of a statically stable system, the response may be transiently unstable due to insufficient damping associated with the PLL [5], [6]. Therefore, to be able to assess the

transient stability of the nonlinear faulted system, EMTDC numerical studies is usually being performed using PSCAD or similar software. However, such an approach includes a high model complexity and computational burden and may be unattractive if many different initial conditions are to be examined. In power systems, the equal-area criterion has been extensively used to asses the synchronization stability of synchronous machines during grid faults. However, system damping is neglected in these formulations which result in a conservative design that may be too conservative considering a power electronic converter where its damping is not constrained be any physical properties. Along these lines, although the static network instability and the small-signal instability associated with the PLL are both well understood, literature is lacking understanding and systematic assessment methods for transient synchronization stability considering the nonlinear effects of the system. This paper, therefore, presents a systematic approach to assess the transient stability of a grid-following converter exposed to a severe grid fault.

II. System Analysis

The setup considered in this paper is depicted in Fig. 1, which consists of a renewable energy source tied to the grid through a grid-following converter exposed to a severe fault at v_F. A third-order LCL filter is used to attenuate the switching harmonics of the converter and a grid-following control structure is employed where the injected currents to the grid is tightly regulated using a stationary-reference frame Proportional-Resonant (PR) controller. As the $\alpha\beta$ current references are oriented by the Synchronous-Reference Frame (SRF)-PLL, the stability of this is important and as will be shown, in particular during severe grid faults. The external network contains a line impedance and a parallel feeder branch where the upper branch is represented as a Thevenin equivalent and the lower feeder will be exposed to a three-phase symmetrical fault where Z_f represent the feeder and fault impedance.

Assuming a solid fault to occur very close to the v_F bus where $Z_f << Z_{th}$, then the power flow during the fault can be accurately described from a single-line diagram where the

Fig. 1. Structure of grid-tied converter during a power system fault where the fault location is denoted as v_f and the actual short-circuit occurs at the red arrow. A grid-feeding control structure consisting of a SRF-PLL and inner current controller is used for the analysis.

TABLE I
MAIN PARAMETERS OF THE SYSTEM IN FIG. 1

Symbol	Description	Value
S_b	Rated power	7.35 kVA
V_b	Nominal grid voltage (l-l, rms)	400 V
V_{dc}	dc-link voltage	650 V
f_0	Rated frequency	50 Hz
f_{sw}	Switching frequency	10 kHz
f_s	Sampling frequency	10 kHz
L_{cf}	Converter-side inductor	0.07 pu
L_{gf}	Grid-side inductor	0.04 pu
C_f	Filter capacitor	0.07 pu
K_{pc}	Current controller K_p	12
K_{rc}	Current controller K_r	2000
K_p^*	Initial PLL Design of K_p	0.195
K_i^*	Initial PLL Design of K_i	6.2

power transfer is determined by the voltage at the PCC, v_F, and the line impedance $Z_L = R_L + jX_L$. Using this, then for a given current injection, the voltage at the PCC can be described as

$$\boldsymbol{v_{PCC}} = V_F e^{j\theta_g} + Z_L I_{PCC} e^{j(\theta_c + \phi_c)} \qquad (1)$$

where θ_g is the angle of the sagged grid voltage, $\theta_c = \theta_I + \theta_{PLL}$ is the phase-angle of the injected current based on the estimated phase-angle of the PLL, $\theta_I = \tan^{-1}(I_q^*/I_d^*)$, ϕ_c is the impedance angle of the line impedance, and Z_L is the magnitude of the line impedance. Reformulating this such that it is seen relative to the rotating frame of the PLL, the imaginary part of the PCC voltage becomes

$$v_q = Z_L I_{PCC} \sin(\theta_I + \phi_c) - V_F \sin(\delta) \qquad (2)$$

where $\delta = \theta_{PLL} - \theta_g$. As it can be seen from (2), for the PLL to be capable of regulating the q-axis voltage to zero, then [7]

$$I_{PCC} \leq \frac{V_F}{Z_L|\sin(\theta_I + \phi_c)|}. \qquad (3)$$

The issue of loss of synchronization usually happens during weak grid and fault conditions. According to the grid codes, during a severe fault, the injected reactive current should be nominal. Doing this while assuming the converter to only inject reactive current, $\theta_I = -90°$, then the stability limit for the injected current magnitude reduces to $I_{lim} = V_F/R_L$. From this, one can see that the static network limitation during reactive current injection is exclusively depending on the fault voltage magnitude and the line resistance. However, even with the constraint in (3) being satisfied, instability may occur due to the nonlinear dynamic response of the synchronization process. Therefore, the remainder of this paper presents a systematic approach on how to correctly assess the transient stability of this system and how to design and plan for stability during severe events.

A. Initial Design of SRF-PLL

The measured PCC voltage can be expressed in the synchronous dq-reference frame as $\boldsymbol{v_{PCC}} = \boldsymbol{v_{PCC}^s} e^{-j\theta_{PLL}}$ where superscript s denotes that the complex space vector is expressed in the stationary $\alpha\beta$-reference frame. θ_{PLL} is the estimated PLL phase-angle of the voltage used to perform the Park transformation. Expanding the expression for the PCC voltage, one can write the q-axis component as

$$\begin{aligned} v_q &= V_{PCC} (\sin\theta_{PCC}\cos\theta_{PLL} - \cos\theta_{PCC}\sin\theta_{PLL}) \\ &= V_{PCC}\sin(\theta_{PCC} - \theta_{PLL}) = V_{PCC}\sin(\Delta\theta). \end{aligned} \qquad (4)$$

where V_{PCC} is the magnitude of the PCC voltage vector, θ_{PCC} is the actual phase-angle of the PCC voltage, and $\Delta\theta = \theta_{PCC} - \theta_{PLL}$ is the phase error between the actual and estimated phase angle. Using the small-angle approximation, this can be expressed as $v_q = V_{PCC}\Delta\theta$. The SRF-PLL consists of a nonlinear phase-detector (v_q), a loop filter (a PI regulator), and a voltage controlled oscillator (pure integrator) as it is shown in Fig. 1. From this, the linearized closed-loop transfer function of the SRF-PLL is

$$\begin{aligned} G_{PLL}(s) &= \frac{\Delta\theta}{\Delta v_q} = \frac{V_{PCC}K_p s + V_{PCC}K_i}{s^2 + sV_{PCC}K_p s + V_{PCC}K_i} \\ &\approx \frac{2\zeta\omega_N s + \omega_N^2}{s^2 + 2\zeta\omega_N s + \omega_N^2} \end{aligned} \qquad (5)$$

where ζ is the damping ratio and ω_N is the undamped natural frequency of the system. From this, the undamped natural frequency and damping ratio can be expressed as

$$\omega_N = \sqrt{V_{PCC}K_i} \approx \frac{1.8}{t_r}, \quad \zeta = \frac{K_p}{2}\sqrt{\frac{V_{PCC}}{K_i}}. \qquad (6)$$

where t_r is the rise time of the system. The PLL control parameters are often selected such that its bandwidth is much smaller than the bandwidth of the inner current regulator and with an optimal damping ratio of 0.707. Using this together with a desired rise time of 40 ms and a considered operating point where V_{PCC} is nominal, this particular design is referred to as the initial design throughout this paper and is denoted as K_p^* and K_i^* as shown in Table I.

III. NONLINEAR ANALYSIS FOR TRANSIENT STABILITY

The stability assessment of any nonlinear system can be divided into three separate problems where each individual task should be satisfied for stability to be ensured. These three tasks include:

1) Check for existence of an equilibrium point during fault
2) Check for local stability around the found fixed point
3) Analyze the transient response between the pre-fault fixed point and the locally stable intra-fault fixed point

If all these three checks are verified, the system is stable. However, if a fixed point does not exist during the fault or if the found fixed point is locally unstable, then one does not need to analyze the transient response as instability will occur.

A. Existence of Equilibrium Points

Even though the boundary of stability for reactive current injection from (3) is only determined by the fault voltage magnitude and the line resistance, the dynamical impact of the line inductance and PLL must be included to accurately assess the transient stability of the system. As carefully derived in [8], the converter represented as an ideal current source oriented by the nonlinear PLL dynamics can be expressed as

$$\begin{bmatrix} \dot{x}_1 \\ \dot{x}_2 \end{bmatrix} = \begin{bmatrix} f_1(x_1, x_2) \\ f_2(x_1, x_2) \end{bmatrix} = \begin{bmatrix} x_2 \\ -F(x_1, x_2) - D(x_1)x_2 \end{bmatrix} \quad (7)$$

where $(x_1 = \delta, x_2 = \dot{\delta})$ and

$$D(\delta) = \frac{K_p V_F \cos(\delta)}{1 - K_p I_{PCC} L_L \cos(\theta_I)}, \quad (8)$$

$$F(\delta, \dot{\delta}) = \frac{K_i \left(V_F \sin(\delta) - Z_L(\dot{\delta}) I_{PCC} \sin\left(\theta_I + \phi_c(\dot{\delta})\right) \right)}{1 - K_p I_{PCC} L_L \cos(\theta_I)}. \quad (9)$$

An equilibrium point of the system must satisfy a zero velocity state where (7) equals (0,0). This obviously implies that $x_2 = 0$ and that $-F(x_1, x_2) = 0$. Using the expression for $F(x_1, x_2)$, the fixed point or singular point must satisfy that

$$\frac{Z_L I_{PCC} \sin(\theta_I + \phi_c)}{V_F} = \sin(x_1). \quad (10)$$

Notice here that the magnitude and phase of the line impedance is no longer a function of x_2 since $x_2 = 0$ per definition of the fixed point. This implies, that to satisfy (10), an equilibrium point must satisfy

$$\left| \frac{Z_L I_{PCC} \sin(\theta_I + \phi_c)}{V_F} \right| \leq 1. \quad (11)$$

Considering the converter to inject nominal reactive current during the grid fault ($I_{PCC} = 1, \theta_I = -90°$), the equilibrium point expressed in per unit quantities must satisfy $R_L \leq V_F$ which is in agreement with (3). From this, the equilibrium point during the fault is

$$\boldsymbol{x_0} = (x_{10}, x_{20}) = \left(\sin^{-1} \left(\frac{Z_L I_{PCC} \sin(\theta_I + \phi_c)}{V_F} \right), 0 \right), \quad (12)$$

where x_{10} is periodic with 2π. However, from a practical point of view, there are no distinctions between the points.

B. Local Stability of Equilibrium Point

Before analyzing the transient stability of the nonlinear system, one must assure that the system is small-signal stable at the just derived fixed point as the stability of the linear system is uniquely determined by the characteristics of the fixed point. This is done by checking the eigenvalues of the linearized state matrix of the system. To be able to perform eigenvalue analysis, the system must be linearized around a selected operating point (12), where the variables of the nonlinear system $\boldsymbol{x}$ are represented as a small-signal perturbation around the equilibrium point as $\boldsymbol{x} = \boldsymbol{x_0} + \Delta \boldsymbol{x}$ [9]. From Poincaré and Lyapunov [10], if the linearized system is stable, so is the original nonlinear system sufficiently close to that operating point, given that at least one eigenvalue has a non-zero real part. With this, one can use the analyzing tools from linear control theory and analyze the behavior and characteristics of the system considering the damping and oscillating frequency of the system poles.

Considering the Taylor expansion around an expansion point $\boldsymbol{x_0}$ as

$$f(\boldsymbol{x}) = f(\boldsymbol{x_0}) + f'(\boldsymbol{x_0})(\boldsymbol{x} - \boldsymbol{x_0}) + r(\boldsymbol{x}) \quad (13)$$

and shift the coordinate system to the equilibrium point such that at the expansion point $\boldsymbol{x_0} = 0 \implies f(\boldsymbol{x_0} = 0)$, the linear approximation of the system, where the higher order terms are neglected, reduces to

$$\dot{\boldsymbol{x}} = \boldsymbol{A}\boldsymbol{x}. \quad (14)$$

Here, $\boldsymbol{A}$ is the Jacobian matrix containing the partial derivatives of the system evaluated at the equilibrium point and it is expressed as

$$\boldsymbol{A} = \begin{bmatrix} A_{11} & A_{12} \\ A_{21} & A_{22} \end{bmatrix}, \text{where } A_{ij} = \left[\frac{\partial f_i}{\partial x_j} \right]_{\boldsymbol{x}=\boldsymbol{x_0}}, i, j = 1, 2. \quad (15)$$

Computing the Jacobian for the system evaluated in the derived fixed point in (12) gives

$$\boldsymbol{A} = \begin{bmatrix} 0 & 1 \\ \frac{-K_i V_F \cos(x_{10})}{1 - K_p I_{PCC} L_L \cos(\theta_I)} & \frac{K_i I_{PCC} L_L \cos(\theta_I) - K_p V_F \cos(x_{10})}{1 - K_p I_{PCC} L_L \cos(\theta_I)} \end{bmatrix}. \quad (16)$$

The eigenvalues or system poles are found by solving the characteristic equation, $\det(\boldsymbol{\lambda I} - \boldsymbol{A}) = 0$, which has the solution

$$\lambda_{1,2} = \frac{A_{22} \pm \sqrt{A_{22}^2 + 4A_{21}}}{2}, \quad (17)$$

which is stable for eigenvalues with a strictly negative real part. For this case, the original nonlinear system is locally asymptotically stable, meaning that in some area around the equilibrium point, the solution will converge back to this point as time approaches infinity following a disturbance. However, the size of this area or domain of attraction is so far not known. In the case of a zero real part, the system is a marginally stable oscillating system where the truncated higher-order terms from the Taylor series expansion will have a decisive effect on whether the nonlinear system is stable or unstable. Due to this, the linear stability can only be guaranteed for eigenvalues with

(a) V_F is varied from 0.25 pu (blue) to 0.04 pu (red).

(b) θ_I is varied from $-90°$ (blue) to the fixed point limit of $-40.5°$ (red).

(c) R_L is varied from 0 (blue) to 0.05 pu (red).

(d) K_p is varied from $10K_p^*$ (blue) to 0 (red).
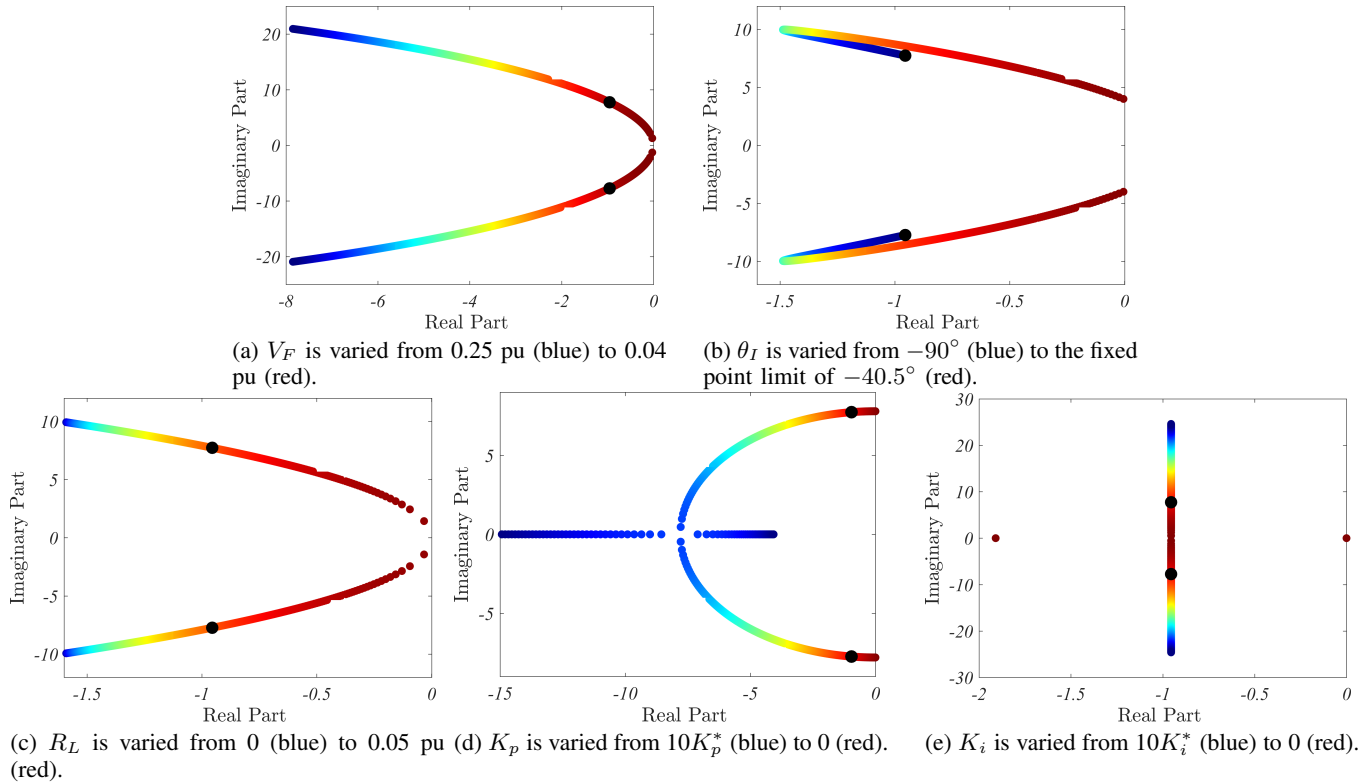
(e) K_i is varied from $10K_i^*$ (blue) to 0 (red).

Fig. 2. Eigenvalues analysis to change in parameters. From blue to red indicates that the poles approach the right-half plane. All plots besides (a) are with $V_F = 0.05$ pu. The black dots on all the sub-figures shows the pole location of the reference system with the initial design.

a strictly negative real part. Considering the converter to inject reactive current, the complex conjugated pole pair will have a negative real part for positive controller gains in the PLL. Considering such eigenvalues, the trajectory of the nonlinear system can be characterized as a stable focus where its solution for a small-signal disturbance will graphically be represented as a shrinking spiral converging towards to equilibrium point x_0.

Eigenvalue analyses where V_F, θ_I, R_L, and the PLL controller gains have been swept are presented in Fig. 2a-2e. From these it can be seen that all eigenvalues for any change in parameters that satisfy the fixed point condition during the fault are located in the left half-plane. It should be perceived that each plot either enters the right half-plane or is located at the imaginary axis when the swept parameter is directly placed on the equality of (11), i.e. at the boundary of the static stability limits. Therefore, from the local stability analysis, the system appears to be quite robust towards parameter changes given that a stable fixed point exists. It should be mentioned that the eigenvalue analysis performed is aiming to identify any low-frequency oscillation modes which may become unstable. In Fig. 2d where the bandwidth of the PLL is altered, the dynamics associated with the inner current regulator should be included for an accurate assessment. Anyhow, as this paper intent to shed light on the low-frequency instability by cause of violation of static network limitations, the contribution of the inner current regulator can be neglected for this analysis

as it is shown in [8].

C. Transient Stability Analysis using Phase Portraits

Even though the system may be stable at the equilibrium points before and during the fault, it is far from certain that the system will actually be attracted to this stable point considering a large-signal disturbance. The nonlinear system stability can be evaluated using Lyapunov's direct method where an energy-like function is used to assess whether the total energy of the system will decrease, meaning that the solution will eventually converge to an equilibrium point. Even though this method is quite elegant and its physical interpretation is straight forward, how to develop such a function is not generally described. As a result of this, such a stability problem is usually approached through transient stability studies where the nonlinear system is solved using numerical methods for a great number of initial conditions. Instead of performing a time-consuming simulation of the detailed simulation model, one can use phase portraits to get a graphical solution for first and second-order nonlinear systems. Using this, one can analyze a large amount of different initial conditions of the faulted system and graphically visualize the trajectory of each solution in the $(x, \dot{x})$ phase-plane for a given initial condition. To be able to say something about the stability boundary, the area of attraction, and determine what damping ratio of the PLL dynamics is sufficient for the trajectory of the system to be attracted to the stable operating point, a large number of initial conditions are solved

using phase-plane plots. For this work, these initial conditions are changed by sweeping the PLL controller gains. From this, one can to a selected numerical accuracy determine the needed damping for the system to ride-through the large-signal disturbance in a stable manner given the existence of a stable operating point during the fault.

The initial conditions for x is described in detail in [8].

IV. Numerical Study of Transient Stability

By implementing the initial conditions alongside the system equations in (7), the critical value for PLL damping which guarantees stability can be found using a sweep of the control parameters of the PLL (K_p, K_i). The PLL damping ratio is calculated as shown in (6). Clearly, an equilibrium point must exist during the fault, hence $V_F \geq R_L$. In Fig. 3a-3f, the trajectories of the system exposed to a grid fault are visualized for different fault voltage magnitudes and values of the proportional gain of the PLL. In the figures, the color code indicate an increased damping ratio of the PLL as one goes from blue towards red.

As can be seen in Fig. 3a, when $V_F = 0.06$ pu, the damping of the initial controller design is sufficient to keep the system stable. However, when the fault voltage magnitude is decreased, a larger damping is required in order for the system to be attracted to the fixed point during the fault. As it can be seen, when V_F approaches $R_L = 0.04$ pu, the required damping increases significantly. According to Fig. 3f, a damping ratio of 13.36 and a PLL bandwidth of 191 Hz are required to stabilize the system when the fault voltage drops to 0.041 pu, approaching the theoretical static limit. Notably, from the small-signal analysis performed in Fig. 2a, the instability of the initial PLL controller design for $V_F = 0.05$ pu cannot be seen. However, as shown in Fig. 3b, the system is actually transiently unstable during this design; thus, the nonlinear equation must be used to detect this.

In agreement with (6), the damping ratio can certainly be increased by increasing the proportional gain of the PLL. Nevertheless, this naturally increases the PLL bandwidth which is undesired for practical implementation since the inner current regulator has a limited bandwidth. Under that circumstance, instability may easily occur if the time constants between the two loops are comparable. Therefore, a more prominent way of increasing the damping ratio seen from an cascaded control stability point of view, is to decrease the integral gain of the PLL. An identical set of phase portraits, as just described for sweeps in K_p, are shown in Fig. 4a-4f where here, the integral gain is decreased to increase the PLL damping ratio. As it can be noticed from the figures, the required damping is the same, no matter whether K_p is increased or K_i is decreased. Differently, for the case of a decreased K_i, the PLL bandwidth is nearly unaffected and is therefore much less likely to cause any harmonic coupling to the inner control loop. To that end, if one keeps decreasing K_i to increase the damping ratio, the problem with a high bandwidth is no longer an issue. If the voltage is approaching the static stability limit, the required damping approaches infinity. This is in full agreement with

what is disclosed in [11] where at the stability limit, an infinite damping is attained by removing the integral action of the PLL. This effectively performs a dynamical collapse as the system order is reduced from two to one. From this, reducing the integral gain seems at first like a more attractive solution for increased damping. However, it may also be undesirable to have a too slow PLL, since one, according to the grid codes, need to settle in about 20 ms. Therefore in the case of phase-angle jumps, the PLL must be able to possess some dynamical properties which may put a lower bound on the integral gain.

A. Verification of Phase-Plane Analysis

To verify the phase-plane analysis, two case studies have been conducted in a detailed simulation model of the system, shown in Fig 5. The simulation results are divided into four subfigures where **a)** is the estimated frequency of the PLL, **b)** are the dq-axes currents referenced to the PLL, **c)** are the dq-axes currents referenced to the actual PCC voltage angle, and **d)** are the three-phase voltages at the PCC. For the verification, two damping ratios from Fig. 3d are considered where from the phase-plane analysis, a damping of 3.35 is sufficient to stabilize the system. As it can be seen from the simulation results, a slightly higher damping ratio is required in the detailed model in order to stabilize the system, i.e. 3.48 instead of the predicted 3.35 (3.9% relative error). As a control designer will always leave some headroom to allow for a certain degree of uncertainty and effects associated with unmodeled dynamics, the use of phase portraits and a reduced-order model for transient stability studies can be considered highly accurate. The experimental verification of Fig. 5 is shown in Fig. 6. As it can be noticed, very similar waveforms are reproduced in the laboratory where the setup used is identical to what is described in [7]. In the lab, however, less damping is required to stabilize the system compared to the detailed simulation model, which may result as the exact reactance and resistance values are difficult to precisely tune in the laboratory. Compared to the phase trajectory in Fig. 3d, the relative error is only 2.4%, supporting the validity of the second-order nonlinear model for assessing synchronization stability of grid-connected converters alongside how the domain of attraction can be estimated using this method.

V. Guideline and Recommendation for Transient Stability Robustness

As it is has been shown in the preceding analysis, whether the system will be transiently stable as a result of a severe grid fault depend on several factors which may be different from one application to another. Despite that, a system designer often has some information or bounds on the short-circuit ratio, X/R ratio as well as expected worst case fault profile of a given system. Typical line impedance values of the installation level, as it is seen in Table II, may be used to estimate such a worst case scenario. From this, it will be possible with the presented approach to select a set of controller parameters for the PLL which permit sufficient damping to ensure large-signal stability. Such a selection must be chosen a bit conservatively
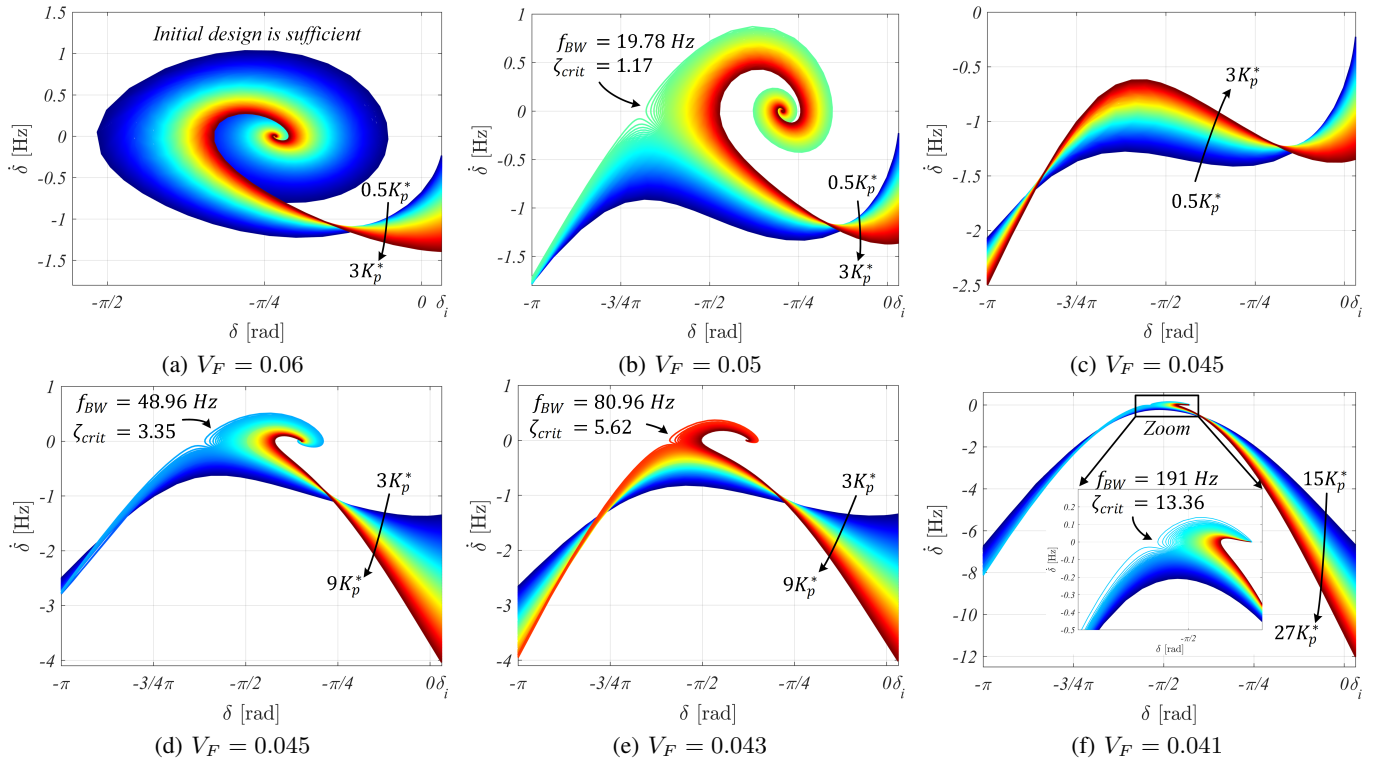
Fig. 3. Phase portraits for a varying K_p. K_p^* denotes the initial PLL design for normal operating conditions. The color code goes from blue to red where the damping increases towards the red graphs. Each sub-figure is shown for 200 different initial conditions.
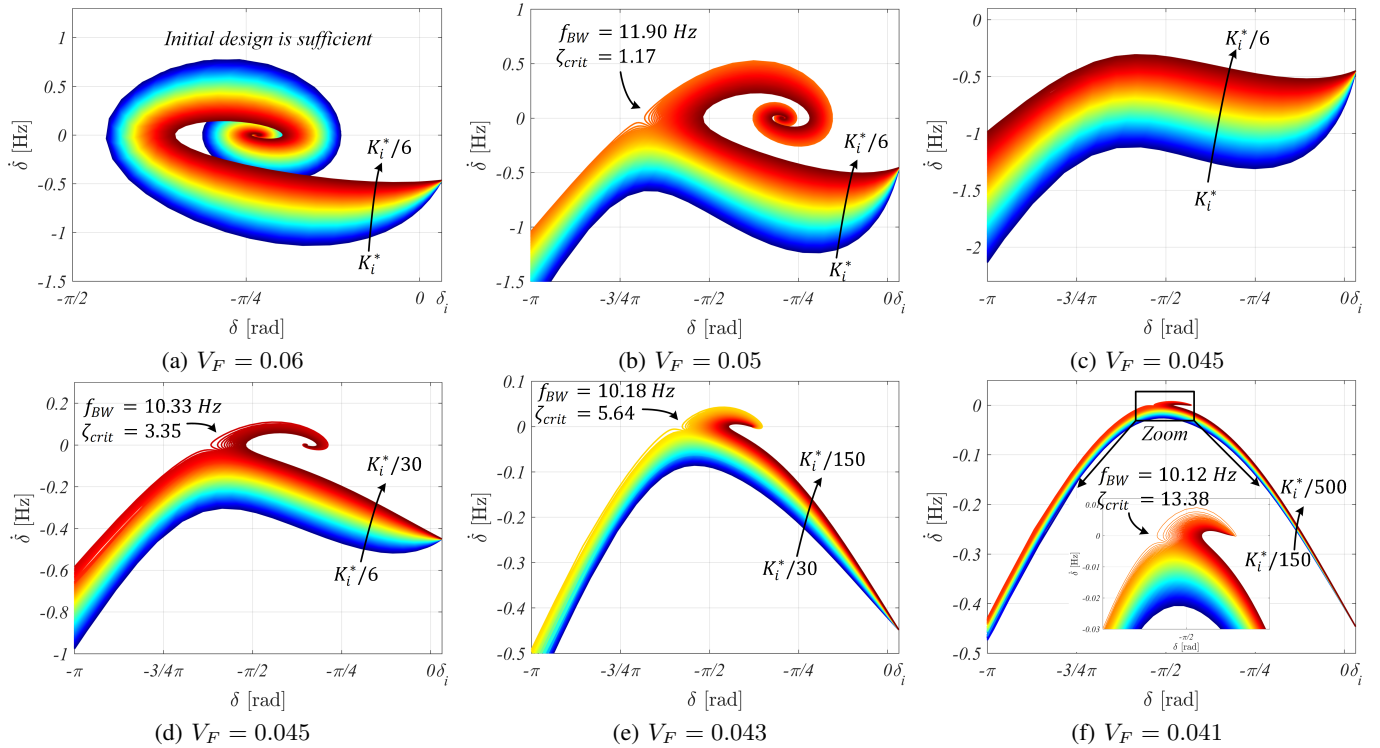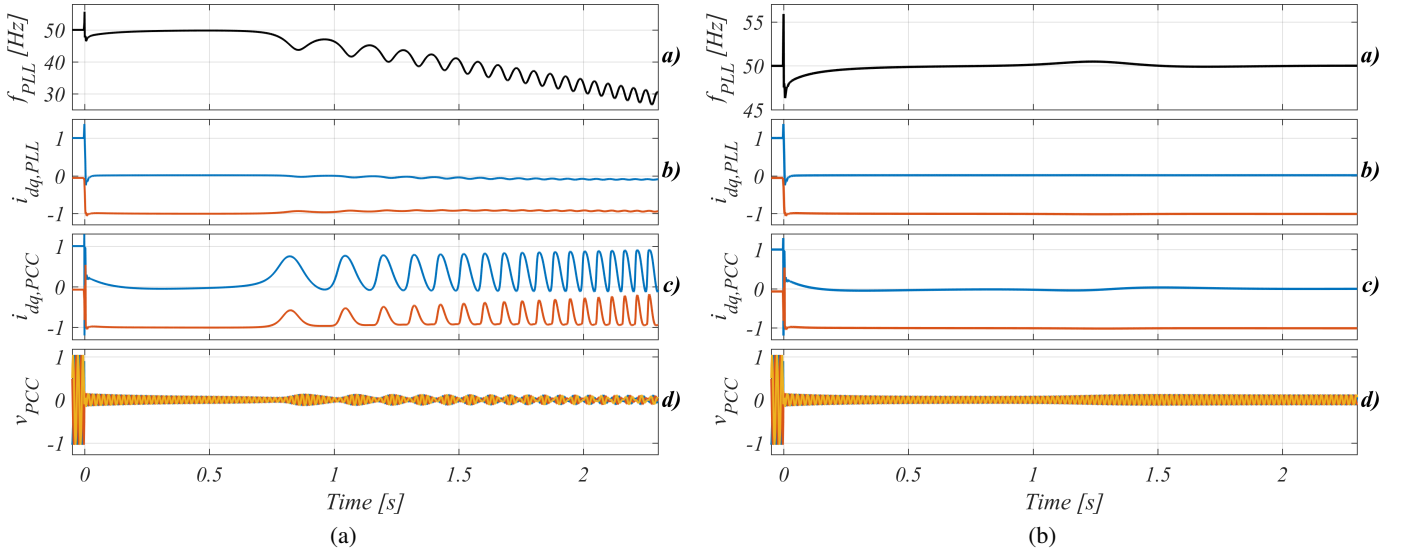

Fig. 4. Phase portraits for a varying K_i. K_i^* denotes the initial PLL design for normal operating conditions. The color code goes from blue to red where the damping increases towards the red graphs.

Fig. 5. Results from detailed simulation model used to verify the developed model implemented with phase portraits. Fig. 3d is taken as an example for the validation. At 0 s the voltage at the fault location drops to 0.045 pu. (a): PLL damping ratio of 3.35 which is unstable. (b): PLL damping ratio of 3.48 which is stable.
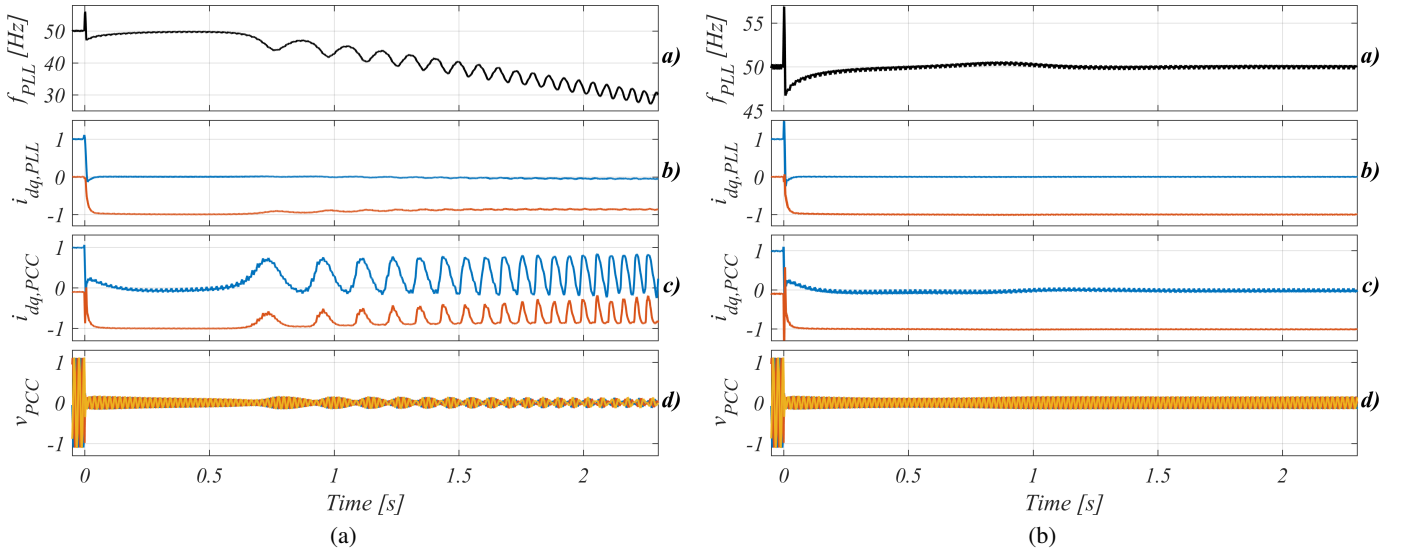
Fig. 6. Experimental results of the cases in Fig. 5. At 0 s the voltage at the fault location drops to 0.045 pu. (a): PLL damping ratio of 2.9 which is unstable. (b): PLL damping ratio of 3.27 which is stable (critically at the tipping point).

to account for any uncertainties and unmodeled dynamics. To that end, the parameters could be applied only when a fault is detected to allow for different designs under normal operating conditions and faults conditions.

In addition to the typical line impedances shown in Table II, much higher X/R values may be present for high-voltage connections. For example, as calculated for a 230-400 kV line in [13, p. 129-140], the X/R ratio can generally also take values in the range $5-20$. From this, it can be seen that as LOS occurs as a result of an imbalance in active power injection, high-voltage networks are more likely to be stable under severe faults since its resistivity is low. When the converter

TABLE II
TYPICAL LINE IMPEDANCE VALUES [12]

Installation level	R [Ohm/km]	X [Ohm/km]	X/R
Low-voltage network	0.642	0.083	0.13
Medium-voltage network	0.161	0.190	1.18
High-voltage network	0.06	0.191	3.18

is connected to a lower-voltage level such as distribution and residential networks, one may expect the instability to be more likely since the X/R value is lower. However, such

an assessment is of course highly dependent on the system topology, length of the lines, a connection of transformers etc. Nevertheless, based on typical line impedance values and different fault locations, a worst-case ratio of V_F/R_L can be estimated. Based on this, the critical PLL damping required for stability can be computed and some margin can be added for increased robustness against estimation and calculation errors.

a) Post-Fault Resynchronization and Protection Relay: At last, it may be possible to imagine a very severe case where the necessary stability condition in (3) cannot be fulfilled. In that case, there do not exist a set of control parameters for the PLL which can stabilize the system. For such a case, as the second-order nonlinear model is clearly representable for analyzing the sub-synchronous loss of synchronization issue, the system designer may use this model to either calculate the critical fault clearing time of the protection relays which operate the circuit breaker or calculate the needed PLL dynamics based on the already predefined clearing time of the relay. In this way, even though the system does not have a stable operating point during the fault, one can ensure that the system will resynchronize when the fault is being cleared. Therefore, even though no fault recovery tests were performed in this paper, as the focus is on the applicability of the reduced-order model, the same approach as presented can be used to analyze a realistic case including fault recovery and the possibility for different pre-fault and post-fault networks topologies. Using the descriptions in this section and the presented systematic approach, one can identify the worst-case scenarios of a given system and plan against transient instability using the flow chart shown in Fig. 7.
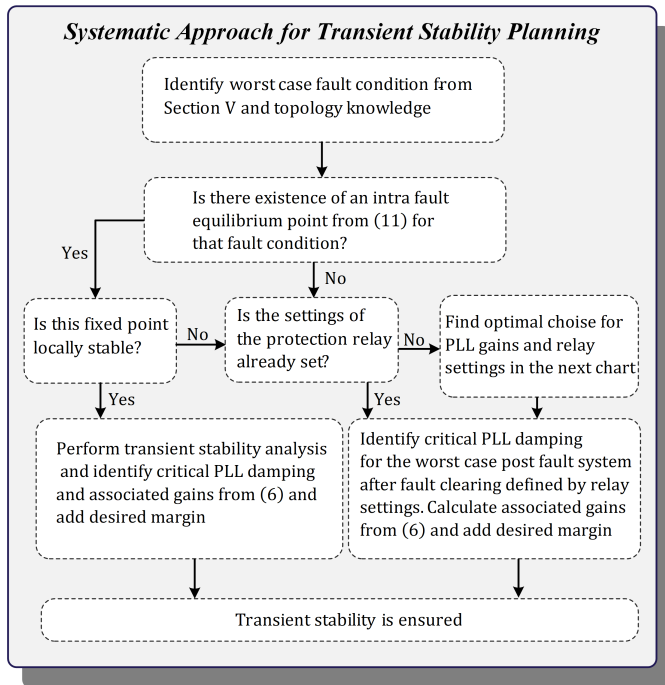

Fig. 7. Flow chart for transient stability planning and PLL gain settings using the systematic approach presented in this paper.

VI. CONCLUSION

During severe grid faults, grid-following converters may be transiently unstable due to insufficient damping associated with the PLL dynamics. To study the transient stability, this paper presents a systematic approach where both the static and dynamic stability of the converter are analyzed. The stability assessment is divided into three individual tasks: checking for existence of equilibrium point during the fault, checking for small-signal stability around that point, and analysis of the transient response between the pre-fault and the faulted operating point. Using phase-plane analysis to analyze the large-signal stability, it has been experimentally verified that it precisely can predict the area of attraction of the state trajectories and associated critical PLL damping ratio during severe faults.

Furthermore, a guideline on how to select the PLL parameters based on usually known network parameters is given in order to ensure transient stability. At last, considering this and a fault condition without a stable fixed point during the fault, a recommendation for planning against transient instability in accordance with the clearing time of the protection relays is given.

REFERENCES

[1] VDE, "VDE-AR-N 4110: Technical requirements for the connection and operation of customer installations to the medium-voltage network (TCC medium-voltage)," 2017.

[2] Ö. Göksu, R. Teodorescu, C. L. Bak, F. Iov, and P. C. Kjær, "Instability of wind turbine converters during current injection to low voltage grid faults and pll frequency based stability solution," *IEEE Trans. Power Syst.*, vol. 29, pp. 1683–1691, July 2014.

[3] I. Erlich, F. Shewarega, S. Engelhardt, J. Kretschmann, J. Fortmann, and F. Koch, "Effect of wind turbine output current during faults on grid voltage and the transient stability of wind parks," in *Proc. IEEE PESGM*, pp. 1–8, July 2009.

[4] D. Dong, B. Wen, D. Boroyevich, P. Mattavelli, and Y. Xue, "Analysis of phase-locked loop low-frequency stability in three-phase grid-connected power converters considering impedance interactions," *IEEE Trans. Ind. Electron.*, vol. 62, pp. 310–321, Jan 2015.

[5] H. Wu and X. Wang, "An adaptive phase-locked loop for the transient stability enhancement of grid-connected voltage source converters," in *Proc. IEEE ECCE*, pp. 5892–5898, Sep. 2018.

[6] M. G. Taul, X. Wang, P. Davari, and F. Blaabjerg, "Grid synchronization of wind turbines during severe symmetrical faults with phase jumps," in *Proc. IEEE ECCE*, pp. 38–45, Sept 2018.

[7] M. G. Taul, X. Wang, P. Davari, and F. Blaabjerg, "An overview of assessment methods for synchronization stability of grid-connected converters under severe symmetrical grid faults," *IEEE Trans. Power Electron.*, pp. 1–1, 2019.

[8] M. G. Taul, X. Wang, P. Davari, and F. Blaabjerg, "An efficient reduced-order model for studying synchronization stability of grid-following converters during grid faults," in *Proc. IEEE COMPEL*, June 2019, in Press.

[9] M. Vidyasagar, *Nonlinear Systems Analysis*. Prentice Hall, 2015. ISBN: 978-1-925261-03-5.

[10] M. J. Gibbard, P. Pourbeik, and D. J. Vowles, *Small-Signal Stability, Control and Dynamic Performance of Power Systems*. University of Adelaide Press, 1st ed., 1993. ISBN: 0-13-623463-1.

[11] H. Wu and X. Wang, "Instability effect of pll on voltage-source converters during grid faults: Large-signal modeling and design-oriented analysis," *arXiv:1811.08926*, Nov 2018.

[12] J. Rocabert, A. Luna, F. Blaabjerg, and P. Rodríguez, "Control of power converters in ac microgrids," *IEEE Trans. Power Electron.*, vol. 27, pp. 4734–4749, Nov 2012.

[13] N. Tleis in *Power Systems Modelling and Fault Analysis - Theory and Practice*, Elsevier, 2008.